Current Distribution Measurements in Parallel-Connected Lithium-Ion Cylindrical Cells under Non-Uniform Temperature Conditions

M. P. Klein[*,z] **and J. W. Park**[**,z]

Mechanical and Aerospace Engineering, University of California, Davis, California 95616-5294, USA

Understanding internal state non-uniformity that occurs across the electrodes in large-format Lithium-ion batteries, and among parallel-connected cells, is a critical part of the cell and battery module design process. Two separate groups of parallel-connected 18650 cells were tested using $LiFePO_4/C_6$ (LFP), and $LiNiMnCoO_2/C_6$ (NMC) chemistries. Pulse and full-capacity discharges were performed at various States of Charge (SOC), C-rates, average temperatures, and levels of temperature non-uniformity. Current non-uniformity for the pulse testing was always lower for the LFP group compared to the NMC group. The hottest cell in the LFP group produced up to 40% more current than average, while this was up to 80% for NMC. Conversely, under charge depleting conditions the NMC group experienced less current non-uniformity, and in certain cases provided a nearly uniform current distribution in the presence of non-uniform temperature. The results indicate that higher temperature sensitivity in the impedance of a cell will cause larger current non-uniformity under pulse conditions. However, due to the presence of non-uniform SOC for charge depleting, the Open Circuit Voltage (OCV) versus SOC gradient plays a significant role in dictating the current distribution behavior, where steeper OCVs provide a corrective action that minimizes the effect of the non-uniform impedance.

 [DOI: 10.1149/2.0011709jes]

Manuscript submitted March 20, 2017; revised manuscript received May 12, 2017. Published July 8, 2017.

Understanding the evolution of non-uniform current and temperature that occurs either across the electrodes in Lithium-ion cells and/or among sets of interconnected cells is a critical part of the cell and module design process for Lithium-ion battery packs.[1–3] The issues of non-uniform current and temperature cause a two-way coupled problem. For example, non-uniform current density can cause non-uniform heating, and therefore non-uniform temperature.[4] Additionally, non-uniform temperature causes non-uniform electrochemical impedance across the electrodes of individual cells and/or across cells in a module which will generate non-uniform current density and therefore non-uniform heating.[5–7]

Several studies, particularly at high charge/discharge rates (i.e., above 1C), show single cell temperature differences greater than 20°C.[3,4,8,9] As a result battery thermal management systems (BTMS) must be incorporated into large scale battery packs, particularly in automotive applications where high C-rates are common. Traditionally, the BTMS is designed in such a way that thermal non-uniformity is kept below 5°C throughout the cell, module, and pack.[4] In order to optimize the BTMS to ensure efficient packaging, thermal performance, and proper electrochemical performance, a thermally-coupled spatially-resolved electrochemical model must be used to understand the coupled effects between the BTMS and the electrochemical performance.

In recent years much progress has been accomplished to model the inhomogeneous behavior of large-format cells. Generally, these can be classified as either True Multidimensional Models (TMM) or Distributed Models (DM). The distinct difference being that the TMM treats the electrolyte transport in the electrode in multiple dimensions to include spatial effects.[10–15] In contrast, the DM connects a set of 0D[2,16–21] or 1D[1,22–27] electrochemical sub-models electrically in parallel through the resistance-network which models the current collectors. Interestingly, few recent works have been conducted to provide experimental validation of the internal current distributions within a cell during operation, and even fewer have explicitly studied the effects caused by non-uniform temperatures.[28–30]

Under uniform thermal conditions the current distributions within a cell have been measured by Zhang et al. on a specially designed pouch cell, which used a segmented cathode with shunts on each segment.[28,29] Additionally, Osswald et al. developed a method for modifying commercial cylindrical cells to measure the electrical potential across the electrode length for spatial model validation.[30]

Fleckenstein et al. developed a test system with three 18650 LFP cells connected in parallel, each with varying degrees of thermal insulation, to understand the effect that non-uniform temperature plays in enabling the development of non-uniform State of Charge (*SOC*).[5] Yang et al. studied non-uniform *SOC* buildup between two 18650 LFP cells connected in parallel, where each cell was held at a different fixed temperature.[27] Troxler et al. studied the impedance effects of a NMC pouch cell while placing various temperature gradients through the thickness of the pouch cell.[6] Finally, we previously studied the effects of non-uniform temperatures for a 10Ah NMC pouch cell similar to Troxler's study.[7] The non-uniform temperature effect was characterized using DC pulse testing and a two hour long US06 dynamic power schedule. For the DC pulse results we agreed with Troxler (performance improvement with increased gradient), but we observed continual buildup of average cell resistance (performance reduction) for the US06 charge depleting test.

We have constructed a new system that can measure the current distribution among five 18650 size cylindrical cells electrically connected in parallel. Additionally, a linear temperature profile may be controlled across the five cells, to study the effect that varying degrees of thermal non-uniformity have on the current distribution under various electrical loading conditions. It is the purpose of this study to provide experimental data to continue to build our understanding of the performance effects caused by non-uniform temperature, and to further advance the validation of spatially-resolved thermal-electrochemical models. The specific ability to measure the current distribution among parallel-connected cells is the key novelty to this study over our previous study, as this now allows for the direct measurement of the amount of non-uniform utilization that results from an applied non-uniform temperature. Additionally, we have studied how this effect differs between the $LiFePO_4/C_6$ and $LiNiMnCo_2/C_6$ cell chemistries.

Separate cell groups using five $LiFePO_4/C_6$ 18650 cells, and the other with $LiNiMnCo_2/C_6$ 18650 cells were evaluated. Total temperature differences of 0, 5, 10, and 20° were applied at average cell group temperatures of 15, 25, and 35°C. The cell groups were tested at 20, 50, and 80% *SOC* and C/5, C/2, 1C, and 2C-rates for 10sec constant-current pulses. Finally, full capacity constant-current discharges were also performed at rates of C/5, C/2, and 1C.

*Electrochemical Society Student Member.
**Electrochemical Society Member.
[z]E-mail: mpklein@ucdavis.edu; jwpark@ucdavis.edu

Background

The key physics in a Li-ion batteries that affect the impedance response are: i) ohmic losses from current collector and tab conductivity, electrolyte conductivity, and, film and contact resistances, ii) charge transfer kinetics, and iii) mass transfer losses due to the ionic diffusivity in the electrolyte and solid phases. The ohmic sources will appear at frequencies faster than 1 kHz, the charge transfer kinetics typically faster than 0.25–10 Hz, the electrolyte mass transfer losses are slower than 0.2 Hz, and finally the solid phase diffusion loss responses are typically much slower than 0.1 Hz.

Andre et al. provide a review of typical impedance spectra and time constants for Li-ion cells.[31] The charge transfer kinetics response time occurs on the order of 1–10 Hz for $LiFePO_4$ and LiC_6, depending on temperature,[32–34] while for $LiNiMnCoO_2$ this is usually slower, and on the order of 0.5–1 Hz.[35–37] Additionally, the charge transfer kinetics is well documented to follow an exponential Arrhenius temperature sensitivity.[35,38] For sub-10sec pulses, at the *SOC* range studied here in our pulse testing (i.e., 20, 50, 80% *SOC*), the kinetics is the primary contributor to *SOC* sensitivity in the cell impedance. The exchange current density coefficient for the Butler-Volmer kinetics equation provides this *SOC* sensitivity.[36] The solid-phase Li-ion diffusivity can also provide *SOC* sensitivity to Li-ion cell impedance, however, this is not generally significantly observable for the short-time pulses.[39] Moreover, the charge transfer kinetics does contribute a rate sensitivity to the impedance of the cell, which reduces with increasing polarization, as defined by the Butler-Volmer equation.

The electrolyte ionic conductivity and diffusivity are temperature sensitive, and Valoen and Reimers have provided a thorough characterization of these parameters for a representative Li-ion electrolyte composed of EC/ PC/ DMC and $LiPF_6$ salt.[40] Over the temperature range tested in our work (278-318K), a linear temperature sensitivity was fit to Valoen's data with an R^2 value of no less than 0.998 for the conductivity and diffusivity at concentrations of 1 and 1.7 mol/L. It is assumed here that the electrolyte temperature sensitivity is linear.

Based on typical Li-ion impedance behavior the measured short-time pulse current distribution response is primarily controlled by the ohmic, charge transfer kinetics, and electrolyte diffusivity phenomena. As a result we have studied the *SOC*, rate, and average temperature sensitivity to varying degrees of temperature non-uniformity. Moreover, any dependence on rate and *SOC* for short-time pulse testing will most likely be caused by the effects of charge transfer kinetics. The rate and *SOC* sensitivity to temperature non-uniformity will depend on how significant the charge transfer resistance varies with temperature and how large it is relative to the total resistance of the cell. Finally, full charge depleting discharges should then allow for separately studying the effects caused by the development of non-uniform *SOC* among parallel-connected cells.

A conceptual model consisting of a parallel connected set of equivalent circuit models (ECM) is used to aid in explaining the experimental observations, and this is presented in Figure 1. We do not use this conceptual model for explicit numerical analysis here, rather for illustrating two key physical effects that were observed in this study. A general model of three cells connected in parallel is illustrated in Figure 1a. Each cell is modeled as an impedance block in series with a voltage source. The impedance block consists of a resistor, R_o, in series with a parallel connected resistor and capacitor, R_{ct} and C_{dl}. Generally, several serially connected RC groups are needed to accurately match the impedance response of the charge transfer kinetics and diffusion mechanisms, however, one RC group is depicted here for simplicity. The voltage source, U_{eq}, models the full cell equilibrium voltage. The impedance block is generally temperature, rate and *SOC* dependent. The equilibrium voltage source is modeled here as a function of *SOC* only. We have purposefully ignored the equilibrium voltage temperature sensitivity, though that is commonly understood to exist for Li-ion battery electrodes.[41–45] For low C-rate cases the entropic effect may be important to account for. Our future model-based studies aim to include this effect in the analysis, but it is not included in this work.

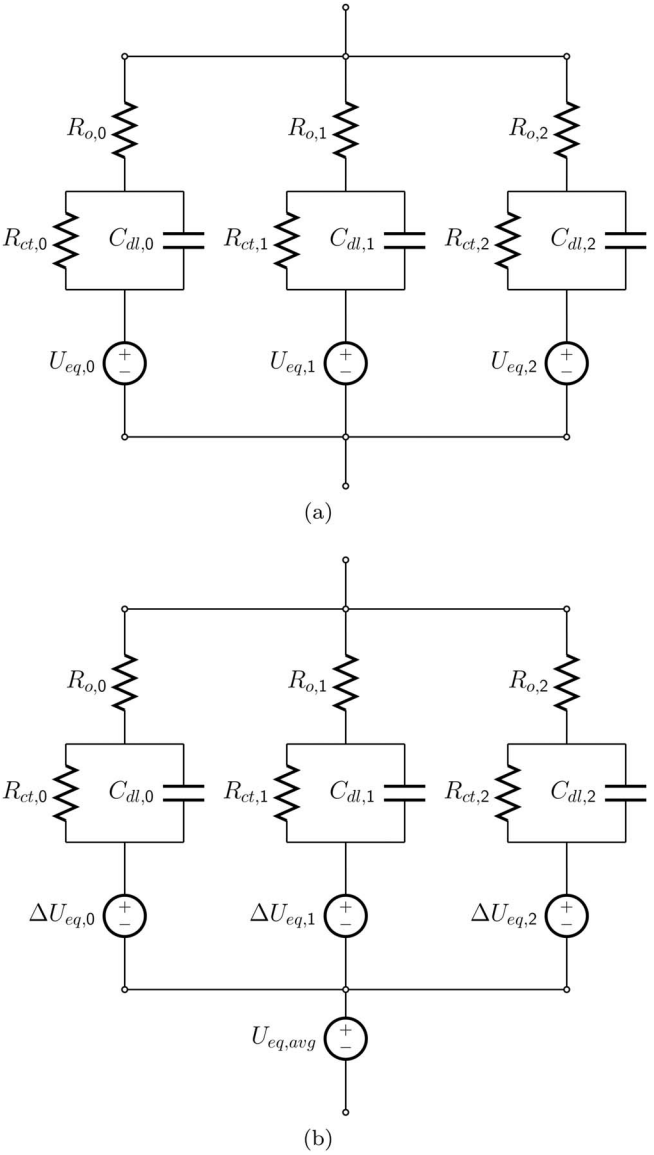

Figure 1. a) General circuit model representation of parallel connected cells. b) Modified representation of the general case in (a), which represents the non-uniformity of equilibrium potential among parallel cells as an additional overpotential.

Figure 1a is rearranged in Figure 1b. This form of the model treats the amount of non-uniform U_{eq} as an additional overpotential. This effective overpotential, ΔU_{eq}, is defined in Equation 1, where $U_{eq,j}$ is the jth cell in the parallel connected set, and $U_{eq,avg}$ is the average equilibrium voltage of the cell group, which is the equilibrium voltage based on the average *SOC* of the cell group. The development of ΔU_{eq} occurs when a non-uniform impedance exists among the cells when current is passed through the cell group, which in the case here is caused by non-uniform temperature. Non-uniform impedance is also be caused by potential gradients along the current collectors, and this effect has been studied recently.[28,30,46–49]

$$\Delta U_{eq,j} = U_{eq,j} - U_{eq,avg} \quad [1]$$

A simplified case where ΔU_{eq} is zero can occur, and in this case the impedance block is the only contributor to non-uniform current. This models the behavior observed in our pulse results, and also the behavior observed in portions of our charge depleting discharge where the slope of U_{eq} versus *SOC* is effectively zero, and thus non-uniform *SOC* cannot cause non-uniform U_{eq}.

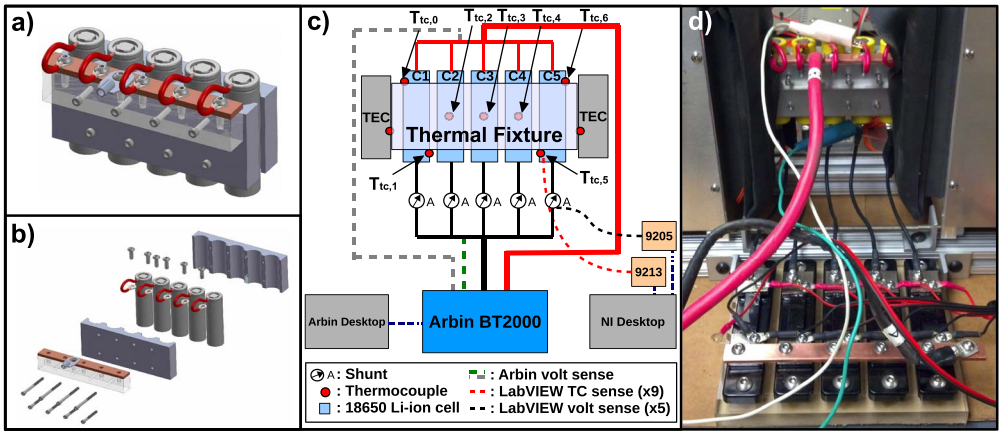

Figure 2. (a) Cylindrical cell fixture. (b) Exploded view of cylindrical cell fixture. (c) Schematic of the full test system. (d) Image of the actual cell/thermal fixture, shunts, and thermoelectric elements.

Methods

Cell specifications.—Five 2.2 Ah NMC and five 1.4 Ah LFP 18650 cells were used for the separate NMC and LFP cell group studies, respectively. All of the cells were nominally rated to provide maximum continuous discharge rates of 3C. For each chemistry ten cells were pulse tested at the same *SOC* and five cells that were within a 2% resistance tolerance were selected as the final cells for a cell group, and this ensured nominally uniform utilization.

System specifications.—*Battery voltage/current data acquisition/control.—*An Arbin BT2000 battery test station was used to apply the electrical test conditions. The Arbin system measured the total voltage and current of the cell group. The individual cell currents were measured using nominally 1.5 mΩ shunt resistors. The uncertainty of the shunt resistance was calculated to 1%. The shunt resistor voltage was measured at a rate of 20 Hz for each shunt using a National Instruments 9205 voltage measurement module. The voltage measurement uncertainty was 0.024 mV. The shunt resistor and voltage measurement uncertainties resulted in current measurement uncertainties of 5.80, 2.49, 1.52, 1.15% for the C/5, C/2, 1C, and 2C-rate tests on the LFP cell group. The uncertainties for the NMC current measurements were 3.77, 1.77, 1.24, and 1.06% for the same respective C-rates.

The five shunts for a given cell group were selected to provide no greater difference in resistance than ±0.5% relative to the shunt group average resistance. The total resistance of the electrical interconnection from the positive busbar to the negative busbar, excluding the cell, was measured to be 3.4 mΩ for the NMC cells, and 8.4 mΩ for the LFP cells. The LFP cells had spot-welded tabs, which contributed slightly more impedance than the soldered joints used on the NMC cells. The additional 3.4 mΩ resistance for the NMC cell group represents at most 8.3% of the NMC cell 10 sec pulse DC-resistance measured at 45°C and 50% *SOC*. For the LFP cell group the relative resistance contribution was at most a 10.5% contribution relative to the 10 sec pulse DC-resistance measured at 45°C and 50% *SOC*. The shunt resistors provided a method to measure the current distribution without significantly affecting the true cell group current distribution when under load.

*Temperature data acquisition/control.—*Each grouping of five cylindrical cells was clamped between two Aluminum blocks with slots machined to capture the cells. Thermal Interface Material was placed between the cells and the Aluminum blocks. Seven thermocouples were attached to the surface of the cells, and their locations are illustrated by the red dots in Figure 2c. Type K thermocouples were connected to a National Instruments 9213 module and a sampling period of five seconds was used. The thermocouples have an uncertainty of ±1°C. The clamped cell group was placed between two thermoelectric temperature control plates (TEC). The TECs were used to control the temperature difference and average temperature across a cell group. The TECs used were the CP-110 model produced by TE-Technology. Each TEC provided continuous fixture edge temperature control during testing. An Oven Industries 5R7-001 temperature controller was used to control the temperature of each TEC. A 24VDC/350W Mean Well power supply provided the DC input power for each of the temperature controllers. A schematic of the system may be seen in Figure 2c and an image of the cell group in the thermal fixture is provided in Figure 2d.

Our system was designed to set a linear temperature profile across the cell group to enable the control of the average temperature and the temperature difference across the cell group. Equation 2 defines the temperature profile, where $T_{tc,k}$ defines the kth thermocouple in a cell group. The individual thermocouples $T_{tc,0}$/ $T_{tc,1}$ and $T_{tc,5}$/ $T_{tc,6}$ measured the left/right edge temperatures of cells 1 and 5, respectively, to enable the measurement of the amount of thermal non-uniformity within a single cell during testing. The single cell temperature difference never exceeded 2°C. Cells 2, 3, and 4 had thermocouples $T_{tc,2,3,4}$ placed at the center of the cell surface. The cell group average temperature, T_{avg}, and temperature difference, ΔT, are defined in Equations 5 and 6, respectively. Our testing approach evaluated the changes in electrochemical performance caused by varying degrees of ΔT at different T_{avg}, C-rates, and State of Charge (*SOC*).

$$\vec{T}_p = \left[\bar{T}_1, T_{tc,2}, T_{tc,3}, T_{tc,4}, \bar{T}_5\right] \quad [2]$$

where,

$$\bar{T}_1 = \frac{1}{2}\left(T_{tc,0} + T_{tc,1}\right) \quad [3]$$

$$\bar{T}_5 = \frac{1}{2}\left(T_{tc,5} + T_{tc,6}\right) \quad [4]$$

$$T_{avg} = \frac{1}{N_{cells}} \sum_{j=1}^{N_{cells}} \vec{T}_{prof,j} \quad [5]$$

$$\Delta T = T_{tc,6} - T_{tc,0} \quad [6]$$

The actual temperature profile deviation from the desired control temperature profile for each test condition was quantified for error analysis. The largest deviations occurred near the end of the full capacity discharge testing, due to increasing cell impedance at low *SOC*. A matrix of the profile errors, which is indexed in time and cell number, was calculated using Equation 7, where $\vec{T}_{p,j}$ is the temperature array of the jth cell in a cell group indexed through test time, and $T_{d,j}$ refers to the desired temperature for that cell for the desired thermal test condition. This matrix of temperature profile errors was then

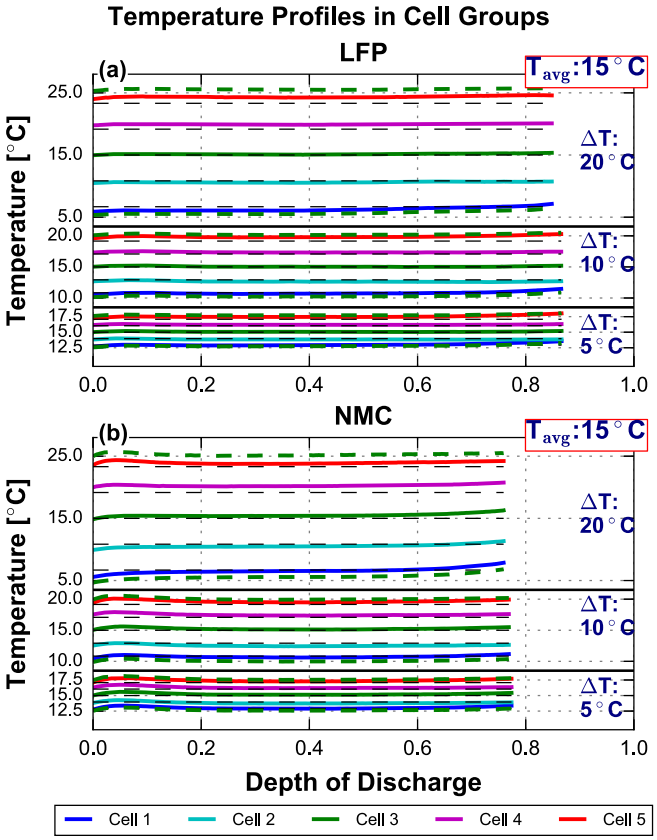

Figure 3. Actual measured temperature profiles for each cell in the cell group (colored lines) compared to the desired constant profiles (black dashed lines) during the Charge Depleting Non-uniform temperature testing. These profiles are for the 1C-rate and 15°C average temperature case. All ΔT conditions are presented. (a) LFP cell group. (b) NMC cell group.

vectorized and the Root-Mean-Square (RMS) error was calculated, as well as the maximum error, and these are defined in Equations 8 and 9, respectively. Here, we use the vec() operator to indicate the vectorization process. This simply indicates the flattening of a matrix to a vector for the error calculations, as is performed in Equations 8 and 9.

$$E_p = \left[(\vec{T}_{p,0} - T_{d,0}), \ldots, (\vec{T}_{p,4} - T_{d,4})\right] \quad [7]$$

$$RMSE_p = \sqrt{\frac{1}{N}\sum_{1}^{N}\left[\text{vec}(E_p)\right]^2} \quad [8]$$

$$MAXE_p = \max\left(\text{vec}(|E_p|)\right) \quad [9]$$

The worst case RMS temperature profile error, $RMSE_p$, evaluated for all test cases was calculated to being 0.9°C. The maximum profile deviation, $MAXE_p$, was measured at 1.7°C, which occurred near the end of the discharges where internal cell heating increased. Therefore, the desired thermal conditions that were applied here remained quite constant, however, the observed deviations may slightly affect the measured current distributions, particularly near the end of discharge for the full charge depleting testing results.

Figure 3 presents the measured temperature profiles for the Charge Depleting Non-uniform temperature testing at the 1C-rate and 15°C average temperature case. This is only for a single test case for each cell group, but this is presented as an example of what the actual temperature profile evolution was during testing. The Charge Depleting data is shown as the temperature profiles did deviate from the controlled condition due to cell heating that occurred over the extend test. The presented subset was the case where the largest temperature profile error was recorded. In subplot (a) the LFP cell group data is presented, and (b) is for the NMC cell group. The line colors represent the cell position in the group, where the blue line is the coldest cell (Cell 1), and the red line is the hottest cell (Cell 5) within the group. The dashed black lines represent the intended control temperature profiles for each cell within the group. The difference between the desired profile and the actual temperature profile was calculated for all measurements as described above using Equation 7. Hence, as detailed in the previous paragraph the error in the desired temperature profile remained within a maximum deviation of 1.7°C, and the RMS error was 0.9°C. These values for the error refer specifically to the 15°C average temperature, 20°C ΔT, and 1C-rate case. The cases at either higher average temperatures, lower ΔT, or lower C-rate experienced lower temperature profile control error, as in those cases the cells generated less heat, and the thermal control system maintained more ideal conditions.

Testing approach.—*Baseline cell characterization.*—The Open Circuit Voltage (OCV) versus SOC curve was generated by averaging C/60 constant-current discharge and charge voltage profiles for both the LFP and NMC cell groups, respectively. Discharging was cutoff at 2.8/2.8 V and charging was cutoff at 3.65/4.2 V for the LFP/NMC cell groups. The OCV test was performed at a uniform temperature of 35°C, and this slightly elevated temperature was used to aid in reducing the cell overpotential.

Following the OCV test the DC resistance (DCR) versus SOC and temperature of the cell group was evaluated under uniform temperature. A 10 sec constant-current C/5 pulses were performed throughout the full SOC window, and at temperatures of 5, 10, 20, 30, and 50°C. The DCR is defined in Equation 10 where V is the measured cell voltage and I_{pulse} is the applied current at the cell level.

$$DCR_{t_{calc}} = \frac{V(t=0) - V(t=t_{calc})}{I_{pulse}} \quad [10]$$

Additionally, the temperature sensitivity of the equilibrium voltage was measured versus SOC. We followed a common testing method used by several others.[41,44] Each cell group cell was brought to a specified SOC, and then allowed to rest for two hours. The temperature was then swept through the following sequence: 45°, 25°, 5°, 25°, and 45° and allowed to rest for two hours at each temperature. The SOC was incremented by 5% for each measurement, and this was evaluated between 75 and 5% SOC.

Non-uniform temperature pulse characterization.—Short 10 sec constant current pulses were performed at three SOCs and these were all run at four C-rates and twelve thermal conditions. This was performed specifically to understand the current distribution response vs. SOC, C-rate, and average temperature when the initial SOC distribution was controlled to be uniform, and does not evolve significantly from that for the duration of the short pulse. Referring back to our conceptual model in Figure 1b, the pulse testing specifically aims to understand the behavior when the ΔU_{eq} terms are zero.

The twelve non-uniform temperature thermal conditions used here consisted of four ΔT (Eq. 6) conditions at 0, 5, 10, and 20°C applied at each of three T_{avg} (Eq. 5) conditions of 15, 25, and 35°C.

Pulse testing evaluated the current distribution for 10 sec constant-current pulses at C-rates of C/5, C/2, 1C, and 2C. The pulse profile for each C-rate consisted of a 10 sec discharge pulse, 30 sec rest, 10 sec charge pulse, and 10 min rest. This full pulse sequence consisted of the pulse profile repeated four times, once for each of the respective C-rates. The discharge and charge pulses were performed at matched C-rates.

The full pulse sequence (i.e., all C-rates) was executed at each of the twelve thermal conditions, and these were all repeated twice in random order to check for consistency. Two hour rests were applied between each full pulse sequence to allow for the new thermal condition to reach equilibrium. The full rate/thermal pulse test was

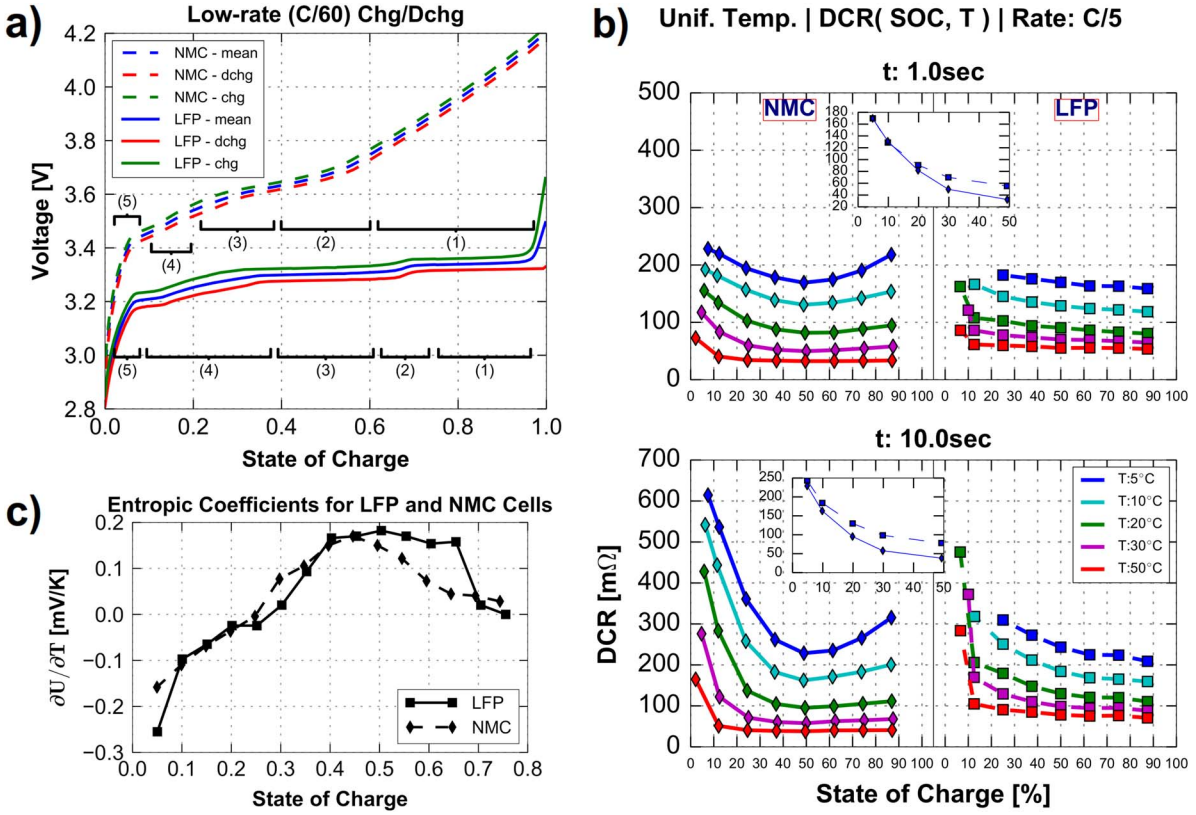

Figure 4. (a) Low-rate (C/60) charge and discharge curves. The averaged curves serve as U_{eq} vs. *SOC* lookup tables, and baseline characterization for modeling. The regions highlighted as (1)-(5) for both chemistries align with the transient phases the current distribution experiences during our charge depleting testing, and this is described in our results section. (b) DC Resistances calculated at 1.0 sec (top) and 10.0 sec (bottom) into a C/5 pulse for the 18650 cylindrical LFP and NMC cells tested in this study. The inset plots show the *DCR* [mΩ] plotted vs. temperature [°C] at the 50% *SOC* point. The inset plots contain lines for both cells, LFP:(- -), NMC:(-). (c) Entropic coefficients for both cell chemistries vs. *SOC*.

performed at 20, 50, and 80% *SOC* to study the *SOC* sensitivity of the current distribution response under pulse conditions.

Non-uniform temperature charge depleting characterization.— Full capacity constant current discharges were performed at three C-rates and twelve thermal conditions. This was performed specifically to understand the current distribution response when the *SOC* does not necessarily remain uniform. Referring back to our conceptual model in Figure 1b, the pulse testing specifically aims to understand the behavior when the ΔU_{eq} terms are no longer necessarily zero. This test allows us to investigate the difference in how varying types of $OCV(SOC)$ sensitivity (e.g., LFP vs. NMC) play a role in controlling the current distribution when a set of cells is placed under non-uniform thermal conditions.

Full capacity constant-current discharges at C-rates of C/5, C/2, and 1C were performed from fully charged to a cutoff minimum voltage of 2.4/2.9 V for the LFP/NMC cell group at the same twelve thermal conditions used in the Non-uniform Temperature Pulse Characterization (Non-uniform temperature pulse characterization section). The rates were chosen to match the rates used in the Pulse Characterization, however, our thermal control system was not able to maintain adequately constant thermal conditions for the 2C charge depleting test.

Results and Discussion

The results are presented in the following order: (i) uniform temperature characterization, (ii) non-uniform temperature pulse (Pulse) characterization, and (3) non-uniform temperature charge depleting (CD) characterization.

Uniform temperature characterization.—The uniform temperature slow-rate and pulse data are plotted in Figure 4 for both the LFP and NMC cell groups. The cell groups provided a total capacity of 7.18 Ah (1.4 Ah per cell) and 11 Ah (2.2 Ah per cell) for the LFP and NMC cell groups, respectively. The slow-rate test was carried out at 35°C and C/60, and this data was used as the full-cell equilibrium potential (U_{eq}) data.

The cell groups were then characterized using a sequence of 30 sec pulses at C-rates of C/20, C/5, and 1C. The *DCR*, calculated at t = 1.0 and t = 10.0 seconds in the C/5 pulse, is presented in Figure 4b. This test was carried out to provide a baseline characterization of the resistance versus temperature of the cells. It is clear that the NMC cells show a larger *DCR* versus temperature and *DCR* versus *SOC* sensitivity compared to LFP.

Finally, Figure 4c presents the sensitivity of U_{eq} to cell group average temperature. We found that the entropic coefficients (i.e., $\partial U/\partial T$) for either the LFP and NMC cells ranged between −0.2 and 0.2 mV/k, depending on *SOC*. These values match well with those found previously for LFP and NMC cells in the literature.[41–45]

Non-uniform temperature pulse characterization.—The 10 sec pulse discharge current distribution response was evaluated across twelve thermal conditions which were all applied at C-rates of C/5, C/2, 1C, and 2C, and three *SOC*s of 80, 50, and 20%. The normalized current ($\hat{I}$) is defined for each cell in a cell group as the cell current divided by the average cell current in the cell group. For example, for the five cell group used here, if the total current draw is 10A then the average cell current is 2A. For a uniform impedance scenario all cells in the cell group would each be providing 2A, and therefore each cell would have a normalized current of one (i.e., 2A/2A). Equation 11 provides the mathematical definition of the normalized cell current

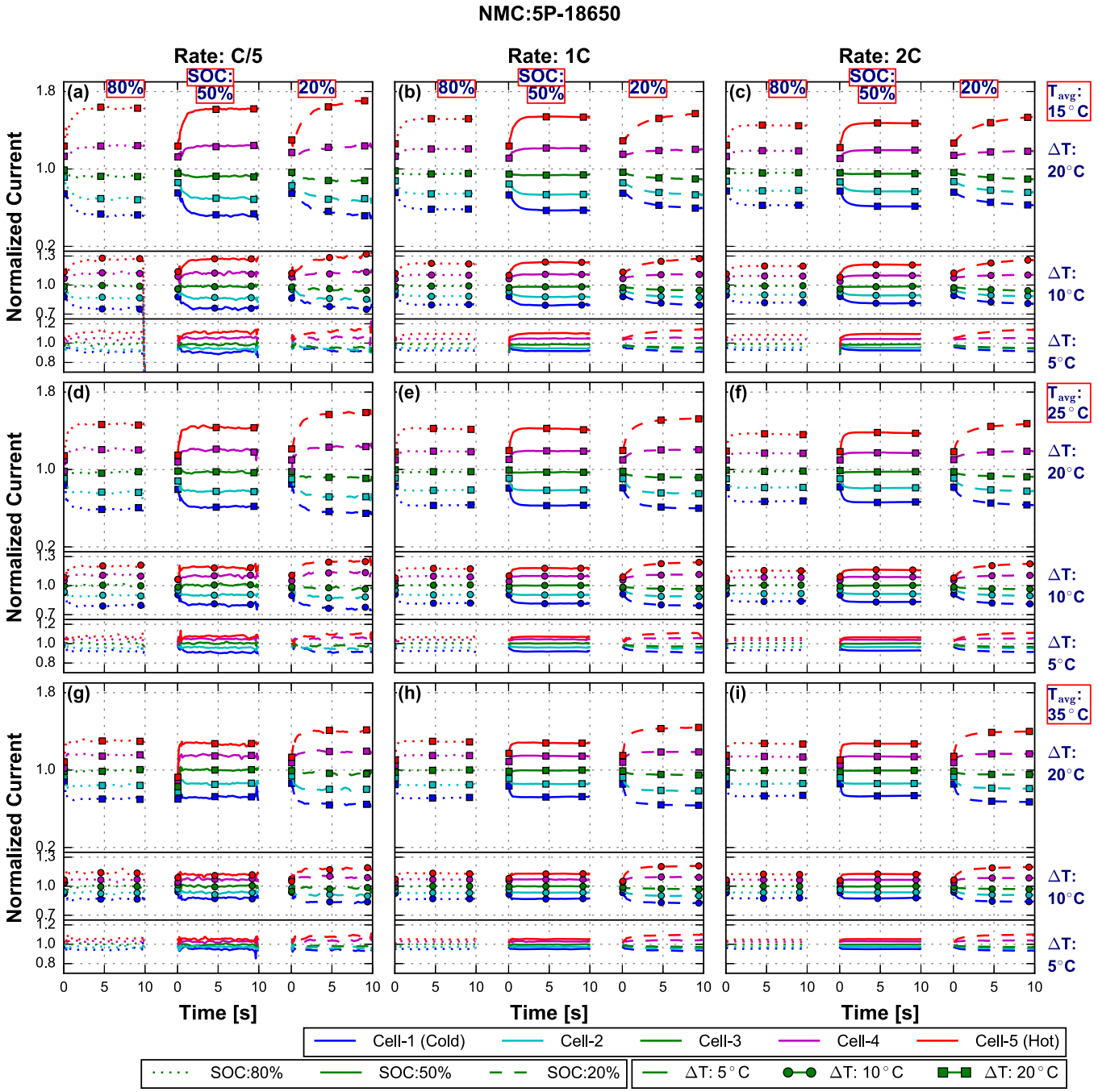

Figure 5. The normalized cell current for all five cells during the 10 sec pulse for the NMC cell group. Line color indicates the cell position within the cell group. Line marker indicates the different ΔT case. Line style indicates the *SOC*. Subplots in the same row refer to the same cell group average temperature; labeled to the right of (c,f,i). Subplots in the same column refer to the same C-rate case; labeled as titles of subplots (a,b,c). Note that the C/2 rate column has been removed to save space. The pulses for the 80%, 50%, and 20% *SOC* cases are plotted in that order from left to right in the same subplot, and these are labeled at the top of (a,b,c).

($\hat{I}_j$), where I_j is the current in the jth cell in the cell group, and N_{cells} is the number of cells in the cell group. This normalized parameter enables the comparison of the current distributions across the different C-rates and cell chemistries tested here.

$$\hat{I}_j = \frac{I_j}{\frac{1}{N_{cells}} \sum_{j=1}^{N_{cells}} I_j} \qquad [11]$$

Figure 5 presents the normalized current distribution responses to the 10 sec current pulse for the NMC cell group. Each subplot contains the normalized current response at 80, 50, and 20% *SOC*, and these are aligned horizontally to each other. Additionally, the response for the 5, 10, and 20°C ΔT conditions are provided in the same subplot, and are aligned vertically to each other. Hence, a single subplot shows the current distribution responses to the 10 sec pulses applied at all *SOC*s and ΔTs at a specified C-rate and T_{avg}. The tested C-rates of C/5, 1C, and 2C are in each column, and the rows of subplots refer to the T_{avg} conditions of 15, 25, and 35°C. Note that the C/2 rate case is not plotted in order to save space, and was removed as it was not substantially different from the C/5 rate case. The plot for the normalized current distribution responses of the LFP cell group is not provided as the current distribution responded at a rate faster

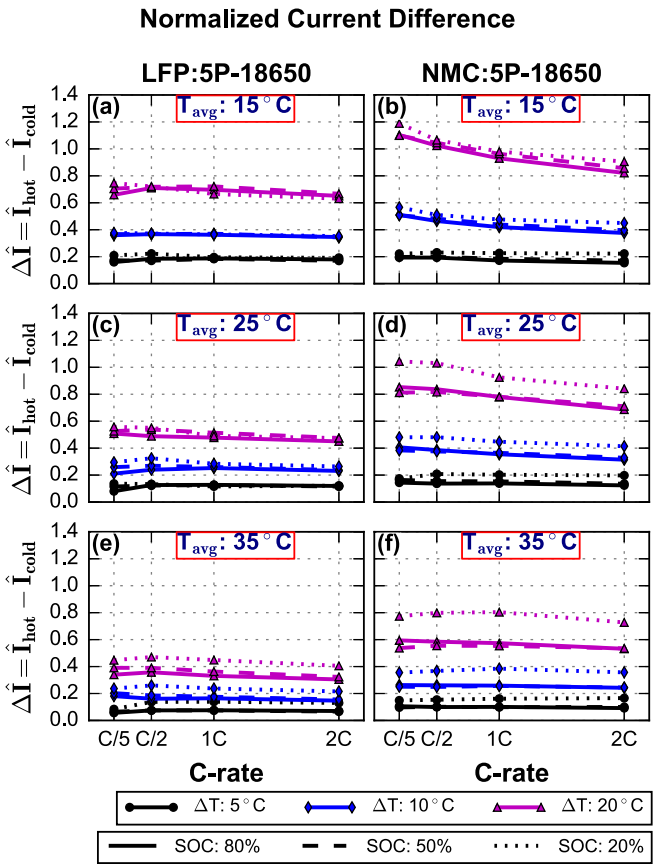

Figure 6. The difference between the hottest (Cell 5) and coldest (Cell 1) normalized cell currents in the LFP (left column) and NMC (right column) cell groups near the end of the 10 sec pulse. Rows refer to the three average temperature conditions tested; from top to bottom: 15, 25, and 35°C.

than 10 Hz, and remained steady for the duration of the 10 sec pulse. The LFP results are more efficiently summarized and compared to the NMC cell group by plotting the total difference in normalized current between the hottest and coldest cells within a group at the end of the 10 sec pulse, which is denoted here as the normalized current difference, $\Delta\hat{I}$, as in Equation 12.

$$\Delta\hat{I} = \hat{I}_{hottest} - \hat{I}_{coldest} \quad [12]$$

There was a noticeable asymmetry in the current distribution for the NMC cell group, and this can be seen most prominently in Figure 5a. This is indicated by the middle cell (Cell 3) having a normalized current less than one. The LFP cell group current distribution was much more linearly distributed among the cells, which indicates that the charge transfer resistance temperature sensitivity was of less significance in the total cell impedance; i.e., the LFP cell resistance is more dominated by linearly temperature sensitive impedance components such as the electrolyte effects.

The normalized current difference between the hottest and coldest cells at the end of the pulse is plotted in Figure 6. The results for both the LFP (left column) and NMC (right column) cell groups is provided to distinguish the differences between the two chemistries. The NMC cell group experienced a larger current difference compared to the LFP cell group for a given ΔT. The rate sensitivity (slope of $\Delta\hat{I}$ vs. rate) increased as either average temperature was reduced, and/or the amount of ΔT was increased. Lastly, the *SOC* effect is also shown. The *SOC* effect was most pronounced at 20% *SOC* and higher T_{avg} for the NMC cell group. Due to the flat U_{eq} (Fig. 4a) and *DCR* (Fig. 4b) vs. *SOC* of the LFP cell group the current difference tended to be insensitive to *SOC*. However, for NMC, which does have a large *SOC* sensitivity at *SOC*s less than 30%, the current difference for the 20% *SOC* case was comparatively more significantly affected. Low *SOC*s cause increases in the charge transfer resistance, and therefore the total resistance would effectively become more temperature sensitive, and this aligns with the increase in current non-uniformity at the 20% *SOC* case for the NMC cell group.

As T_{avg} was reduced the current distribution became more sensitive to ΔT. For example, the LFP cell group at the T_{avg}: 35°C / ΔT: 20°C case produced similar levels of current non-uniformity as the T_{avg}: 15°C / ΔT: 10°C case, which is caused by the Arrhenius temperature sensitivity of the cell resistance. Hence, current non-uniformity is highest when the resistance is most temperature sensitive (i.e., lower T_{avg}). For both cells this occurred at lower average temperatures. For the NMC chemistry this was strongest and also most exacerbated at low *SOC*.

Referring to Figure 6, increases in C-rate caused the total difference in current between the hottest and coldest cells to be reduced. This trend occurred for both the LFP and NMC cell groups, though the effect was more pronounced for the NMC cell group. This can be explained by a situation where the ratio of charge transfer resistance to total resistance, R_{ct}/R_{tot}, is greater in the NMC cell than the LFP cell. Therefore, this would produce a greater rate sensitivity for the total cell resistance.

There was a slight amount of *SOC* sensitivity to the current distribution for the LFP cell group, however, this was primarily observable at the T_{avg} : 35°C case, and even there was quite subtle compared to the NMC cell group *SOC* sensitivity. At the T_{avg} : 25 and 35°C cases the NMC cell group showed a significant change in the overall level of current non-uniformity at the 20% *SOC* case compared to the 80 and 50% *SOC* cases. The 80 and 50% *SOC* pulses were similar, though a slightly smaller current non-uniformity was observed for the 50% *SOC* pulses. The *SOC* effect on the end of pulse normalized current difference was most pronounced at higher average temperatures.

Overall, for both chemistries, the total normalized current difference was highest when the cell impedance was more temperature sensitive, and this tended to occur at lower *SOC*, lower C-rate, and/or lower average temperature. At 20% *SOC*, T_{avg}: 15°C/ ΔT: 20°C, and C/5 the hottest cell in the NMC cell group was required to carry nearly 80% higher current than the average cell current. In comparison, at the same condition, the hottest cell in the LFP cell group carried 40% greater current than the average cell current. This behavior indicates that for pulse conditions the LFP cells have a lower sensitivity to temperature non-uniformity compared to the NMC cells. Additionally, under pulse conditions then, the hotter cells in a module (and/or hotter portions internal to a cell) may be required to charge/discharge beyond design limits when operating near the design limits while experiencing non-uniform temperatures.

Non-uniform temperature charge depleting characterization.— In this section we present the current distribution results for the full Depth of Discharge (DOD) charge depleting discharges. The amount of non-uniform *SOC* and U_{eq} that developed is quantified, and the differences between the current distributions in the pulse and charge depleting cases are compared. Lastly, the consequences that non-uniform temperature has on cell and battery pack designs are considered.

Current distribution behavior.—Figure 7 presents the current distribution behavior of the LFP cell group. Referring to Figure 7g the transient nature of the current distribution is summarized. The LFP cell group goes through at most five phases throughout the discharge. In the first phase there was an initial expansion and then steady distribution, which tended to occur between 0 and 20% DOD. The second phase contracted and then expanded quickly, between 20 and 30% DOD. The third phase was again a steady distribution, where the hotter cells were the stronger contributors to the current. This ranged between 30 and 60% DOD. In the fourth phase, ranging from 60 to 90% DOD, the current distribution experienced an inversion, where the colder cells became the dominant contributors. Finally, from approximately 90% DOD until the end of discharge the current distribution in the fifth phase experienced a rapid expansion and remained in the inverted

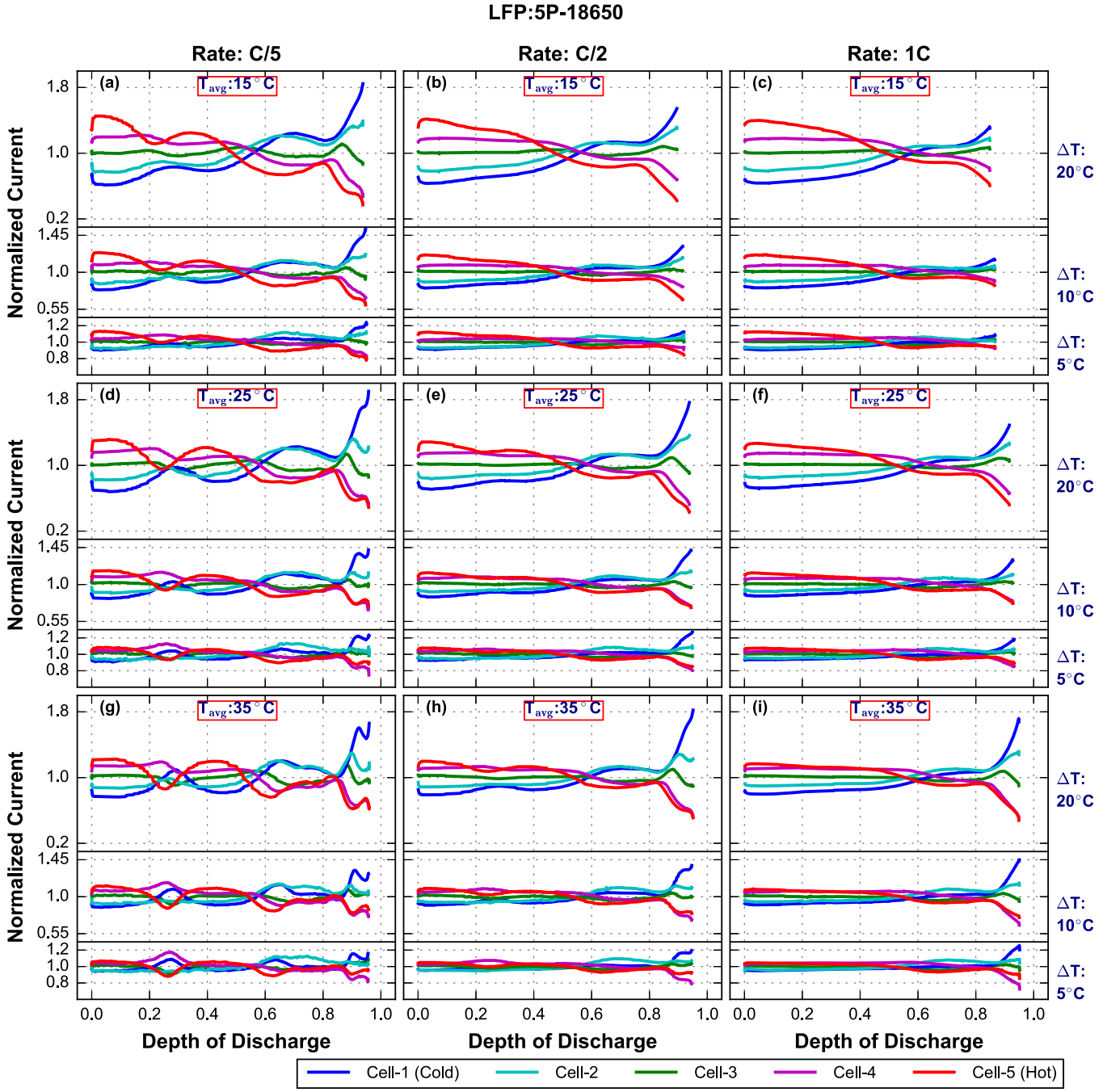

Figure 7. The normalized cell current for all five cells during the full capacity discharge for the LFP cell group. Subplots in the same column refer to the same C-rate case, which are labeled as titles of subplots (a-c). Rows refer to cell group average temperature.

distribution. For visual reference, these phases are highlighted in Figure 4a, as they correlate well with the gradient peaks in the U_{eq} versus *SOC* curve.

Generally, as T_{avg} was lowered and/or C-rate was increased (i.e., overpotential was increased) the current distribution became less dynamic. For example, in Figure 7c (T_{avg}: 15°C and 1C rate) the first three phases tended to merge into one. At higher rates, effective smoothing of the equilibrium potential occurs due to porous electrode effects, and the impedance overpotential becomes more dominant.

It is interesting to compare these results with those of Zhang et al.,[28] where they measured the current distribution among segregated LFP cathodes in an LFP/graphite pouch cell. The cause of the non-uniform current distribution in their cell was due to the potential gradients generated along the length of the current collector. Similar to our results, at low overpotentials, either generated by higher operating temperature and/or lower C-rate, they observed a more transient current distribution throughout the discharge process, and these correlate with the U_{eq} gradient peaks. However, a key difference observed between our study and theirs is that as Zhang increased average temperature, a significant increase in current non-uniformity, $\Delta\hat{I}$, was observed. In Zhang's cell, the source of non-uniform impedance was the current-collector, which had a relatively small temperature sensitivity compared that of the electrochemical impedance. Yet, in our system the non-uniform impedance became less pronounced as average temperature was increased, which is due to the Arrhenius nature of the Li-ion cell impedance. Therefore, higher operating temperature

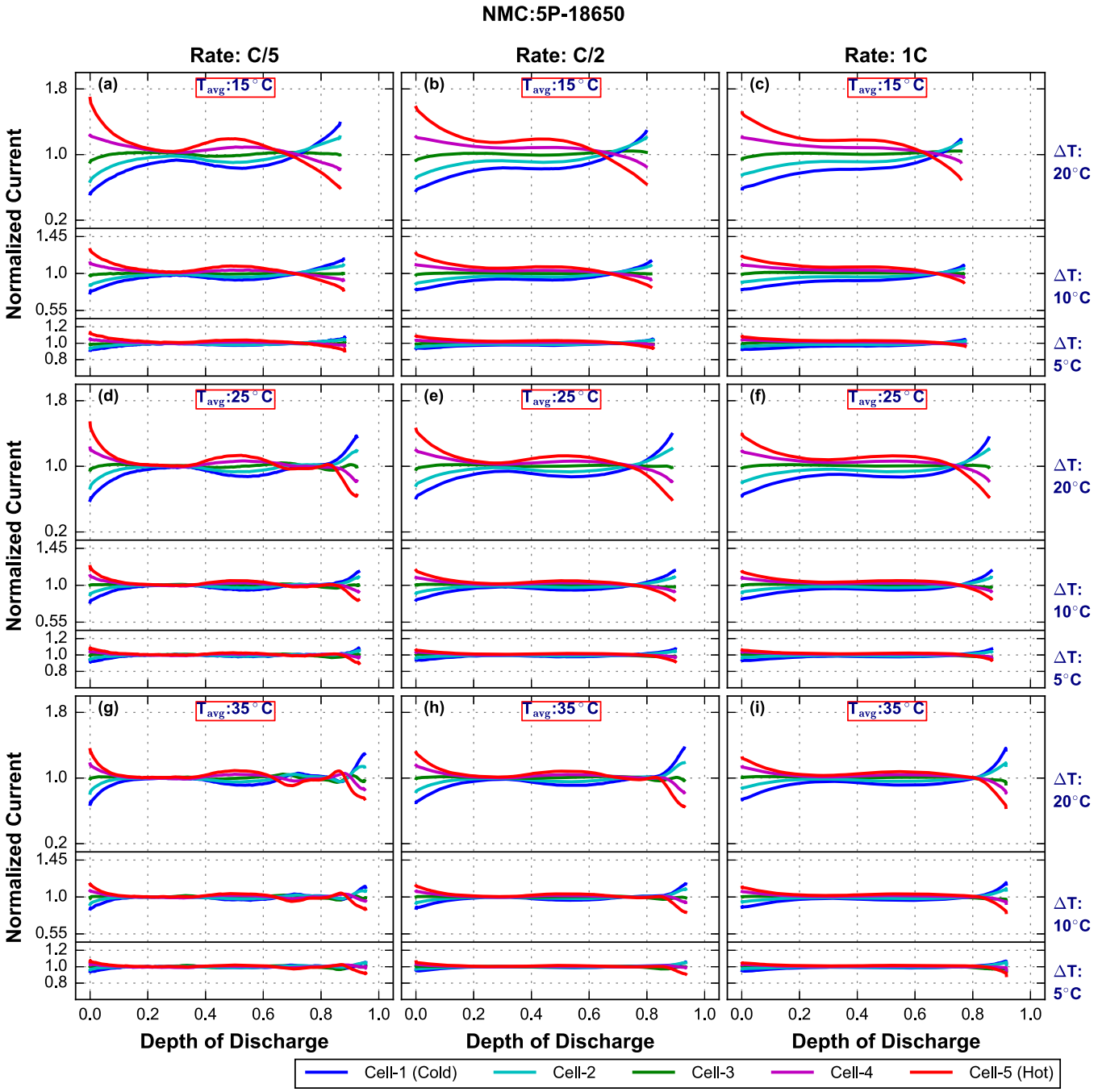

Figure 8. The normalized cell current for all five cells during the full capacity discharge for the NMC cell group. Subplots in the same column refer to the same C-rate case, which are labeled as titles of subplots (a-c). Rows refer to cell group average temperature.

aids in reducing a cells sensitivity to non-uniform temperature, but this conversely increases the negative impacts caused by the potential gradients in current-collectors.

Figure 8 presents the current distributions for the NMC cell group. Referring to Figure 8g the transient nature of the current distribution is summarized. The initial current distribution immediately progressed as a contraction, which fully collapsed to a uniform current distribution, and this spanned between 0 to 40% DOD. In the second phase an expansion/contraction occurred between 40 to 70% DOD, and that corresponds to the point in the U_{eq} curve where the NMC cathode equilibrium voltage experiences a significant transition. Additionally, at that point the first step in the graphite equilibrium occurs. The third phase tended toward an inverted one from 65 to 85% DOD, which then briefly transitioned into the fourth phase flipping back to a hot cell dominated distribution from 85 to 90% DOD. Finally, phase five produced a permanent inversion in the current distribution. Additionally, this inversion occurred much later in the discharge than the LFP cell group inversion. As in the LFP cell group, increasing rate increased the porous electrode smoothing effect, and larger relative impedance overpotential which minimized the transient nature of the current distribution for the NMC cell group.

For both cell groups the *SOC* points where the current distribution transitions correlate well with the *SOC* points in the step changing behavior of the full cell equilibrium voltage curve. This indicates that the changing U_{eq} behavior forces a change in the overpotential of the cell, thus driving a change in the current distribution. Due to the

build up of non-uniform *SOC*, the individual cell U_{eq}s will undergo the U_{eq} step change at offset times during the discharge. For the LFP cell group the primary contributor to the step changes in the U_{eq} vs. *SOC* curve was the graphite anode, which contains quick potential changes between its plateaus.[50] Studying the behavior of the LFP cell group aids in developing an understanding of current non-uniformity evolution under charge depleting conditions for cell chemistries with low U_{eq} vs. *SOC* gradients. In contrast to the LFP cell group, the NMC cathode equilibrium potential is the dominant contributor to the U_{eq} slope for the first 70% of the discharge where finally the graphite drop becomes apparent.[51] Finally, as rate and/or average temperature was reduced the largest initial normalized current distribution was generated, which was true for both chemistries; i.e., where there was the largest *DCR* versus temperature distribution.

Non-uniform state of charge.—Both the maximum ΔSOC and End of Discharge (EOD) ΔSOC are presented in Figure 9. Here, ΔSOC is defined as the difference in *SOC* between the coldest and hottest cells at the same point in time, as in Equation 13. The solid and dashed lines refer to the LFP and NMC cell groups, respectively, while the line colors refer to the varying levels of ΔT. The *SOC* for each cell was calculated via integrating the measured individual cell currents through time, and they were assumed to start at 100% *SOC* at the beginning of the discharge. The maximum ΔSOC that occurred throughout the discharge was larger for the LFP cell group than for the NMC cell group. However, due to the earlier current distribution inversion for the LFP cell group, it has a lower EOD ΔSOC, while actually having a greater maximum ΔSOC earlier in the discharge. For both cell groups the amount of ΔSOC increased with increasing ΔT, and the amount of ΔSOC was reduced as the average cell group temperature was increased.

$$\Delta SOC = SOC_{coldest} - SOC_{hottest} \quad [13]$$

It is important to note that after the discharge was completed the non-uniform *SOC* will equilibrate among the cells. The magnitude of $dU_{eq}/dSOC$ as well as the cell impedance will control the rate of *SOC* equilibration. We did not specifically test to study this effect here, and therefore we do not report on this.

Comparison of the pulse and charge depleting current distribution behavior.—A comparison of the hottest/coldest cell normalized current difference ($\Delta\hat{I}$) between the non-uniform temperature pulse (Pulse) and charge depleting (CD) results is provided in Figure 10. To simplify the plot only the low and high C-rate (C/5 and 1C) and low and high average temperature (15 and 35°C) are presented. The $\Delta\hat{I}$ was extracted from the CD tests at the same average *SOC* point as the Pulse tests (i.e., at 80, 50, and 20% *SOC*). The one exception to this is for the NMC cell group data in Figure 10b, where the end of discharge was reached earlier than 20% *SOC*, and therefore we plot the normalized current difference for the last available *SOC* in that case. The two chemistries are plotted together side-by-side in each subplot for the same respective case. The solid lines refer to the normalized current differences for the CD data, and the dashed lines are for the Pulse data.

For the LFP cell group, in Figures 10b, 10d at the 80% *SOC*/ 1C rate cases, the current distribution for all ΔTs appeared quite similar between the Pulse and CD tests. However, apart from those two cases for the LFP cell group, the current distribution in the CD cases was always smaller than that measured in the Pulse tests. Additionally, we notice that the inversion in the current distribution only occurred in the CD experiment. The NMC cell group also has a greater relative change in the current distribution from the Pulse to the CD test compared to the LFP cell group.

Using the local *SOC*s for each cell at the cell group's average *SOC* points of 80, 50, and 20% the U_{eq} for each cell was interpolated using the quasi-equilibrium voltage data from the C/60 discharge curves in Figure 4a. The thermal sensitivity of the equilibrium voltage was ignored in the interpolation of the equilibrium voltage. For both cell groups used here this amounts a maximum error of 4 mV for the

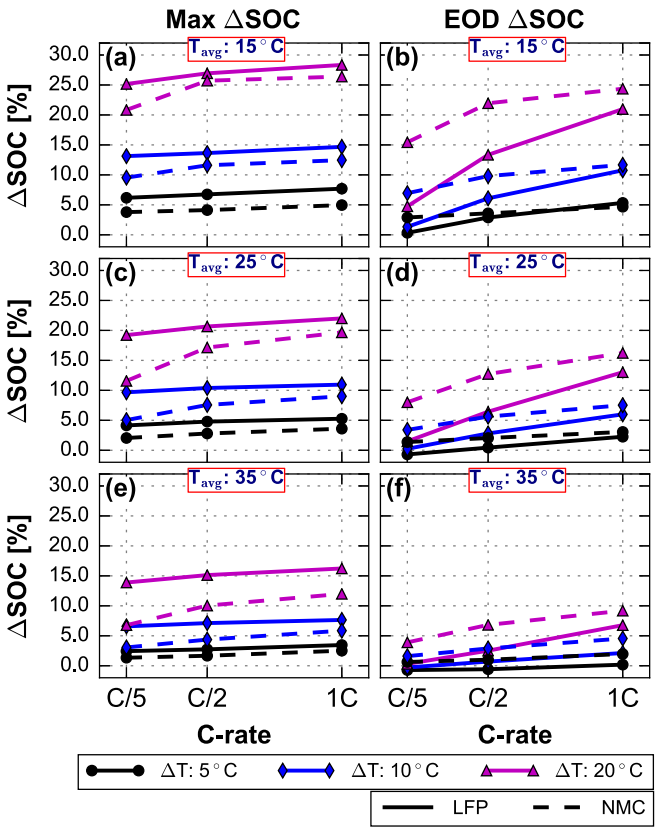

Figure 9. The maximum *SOC* difference (left column) and the End of Discharge *SOC* difference (right column) between the coldest (Cell 1) and hottest (Cell 5) cells in the cell group. Both cell groups are plotted, LFP (–) and NMC (- -), and line color indicates the ΔT condition.

20°C ΔT cases, as the entropic coefficients were measured as being between −0.2 and 0.2 mV/K for the cells used here.

The amount of ΔSOC and the resulting ΔOCV between the coldest/hottest cells is presented in Figure 11. It is important to distinguish the difference between the variables we have defined as ΔOCV and the aforementioned ΔU_{eq}. The ΔOCV term is defined below per Equation 14. These differ in that ΔOCV is the difference in equilibrium potential between the coldest and hottest cells in the cell group, while ΔU_{eq} is defined for each cell in the cell group as the effective overpotential caused by differences in the cell equilibrium potential, $U_{eq,j}$, and the average cell group equilibrium potential, $U_{eq,avg}$ (Eq. 1).

$$\Delta OCV = U_{eq,coldest} - U_{eq,hottest} \quad [14]$$

Referring to Figure 11 we now discuss our reasoning behind the differences in the Pulse versus CD results. Due to the initially flat OCV curve of the LFP cell group, the ΔOCV was less than 5mV, even though the ΔSOC at this point was larger than that of the NMC cell group. Using the cell group terminal voltage (not shown here) the resistance overpotential for the LFP cell group was measured at approximately 200 mV at 80% *SOC*, which was approximately two orders of magnitude greater than the ΔU_{eq} overpotentials. For the same case, the NMC cell group overpotential was measured at approximately 300 mV, while the ΔOCV was on the order of 130 mV for the 20°C ΔT condition. In that case the ΔOCV (and therefore the ΔU_{eq} overpotentials) was of large enough magnitude to play a significant role in controlling the current distribution. Conversely, at 80% *SOC* for the low overpotential cases (e.g., C/5 and 35°C) the impedance overpotential for both cells was only on the order of 25 mV. This then only requires a ΔSOC of less than 3% for the NMC cell group to generate a ΔOCV on the same order as the overpotential.

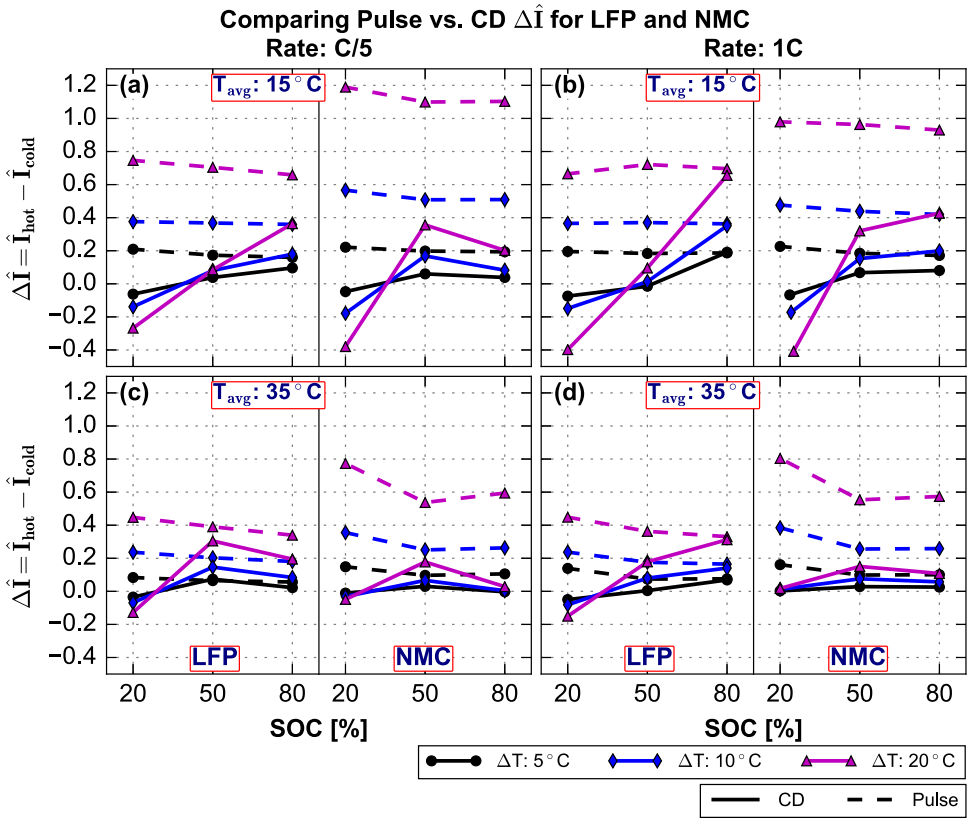

Figure 10. Comparison of the normalized current difference ($\Delta\hat{I} = \hat{I}_{hot} - \hat{I}_{cold}$) between the Pulse and Charge Depleting cases at the same *SOC* points of 80, 50, and 20%. Results shown side-by-side for the LFP and NMC cell groups in the same subplot. To simplify the presentation of the large study only the high and low average temperatures, and the high and low C-rates are plotted here.

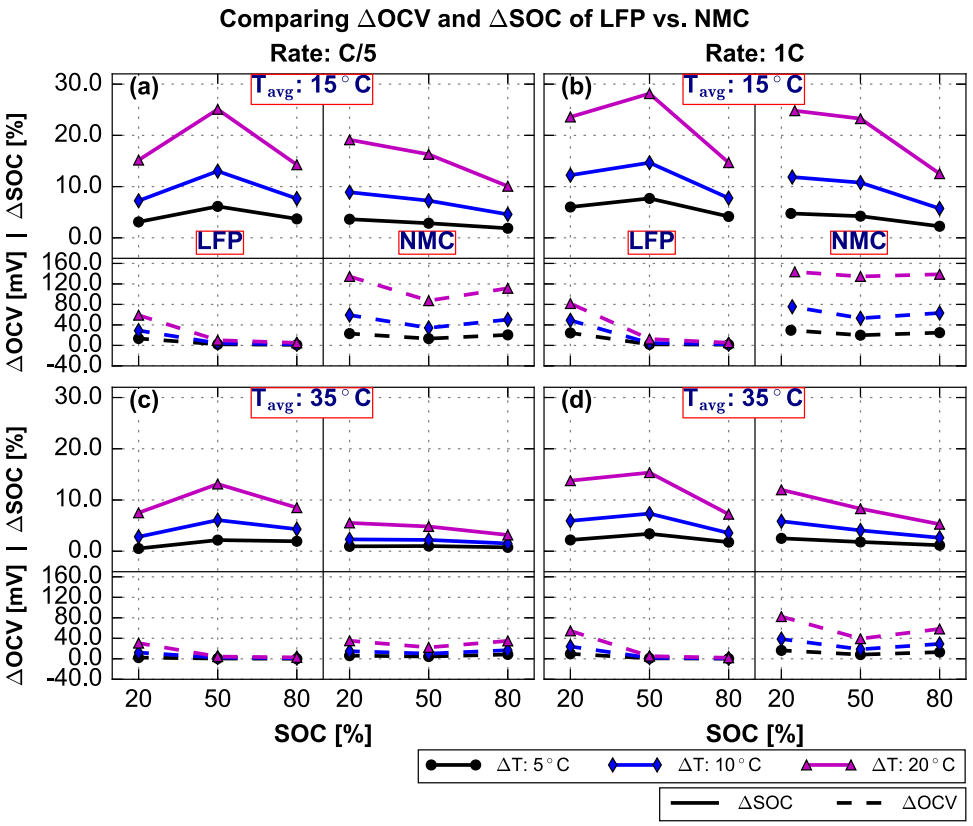

Figure 11. Comparison of ΔSOC and ΔOCV. Results shown side-by-side for the LFP and NMC cell groups in the same subplot. To simplify the presentation of the large study only the high and low average temperatures, and the high and low C-rates are plotted.

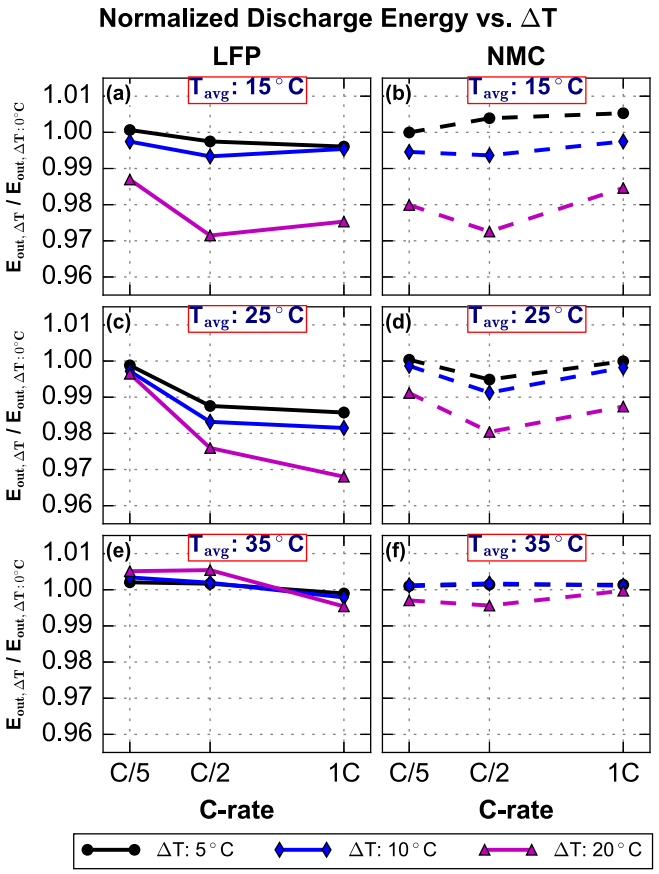

Figure 12. Comparison of the normalized discharge energy between LFP and NMC cell groups. This is showing the effect that ΔT has on the available discharge energy as a function of average cell group temperature and C-rate.

However, the LFP cell group, at 80% *SOC*, would require greater than 30% ΔSOC to develop a 25 mV ΔOCV. Therefore, as we observe at 80% *SOC*, the LFP cell group still experienced a larger current non-uniformity, whereas the NMC cell group was discharging at essentially uniform current. And in general, this was why the NMC cell group had a much more uniform current distribution for the CD testing, even though its current distribution was more non-uniform for the Pulse testing.

Consequences for cell and battery pack design.—We now present extracted system level impacts that the results may have on Li-ion cell and battery pack design. First, we analyze the extracted energy from the individual cells as well as the cell group during the CD discharges. The cell, and then normalize these to their respective ΔT: 0°C case, and this data is plotted in Figure 12. The normalized energy, defined in Equation 15, describes the relative amount of energy discharged from the cell group at a given ΔT condition compared to the same case operated at uniform temperature.

$$\hat{E}_{out} = E_{out}(\Delta T_i)/E_{out}(\Delta T = 0°C) \quad [15]$$

The largest observed relative energy reduction was approximately 3%. This occurred at the T_{avg}: 15°C/ ΔT: 20°C condition for both cell groups at C/2, as well as the T_{avg}: 25°C/ ΔT: 20°C condition for only the LFP cell group. For ΔTs less than 10°C, the NMC cell group never experienced more than a 1% reduction in the normalized discharge energy, while the LFP cell group energy reduction was never more than 2%. These results again indicate that the NMC cells were more tolerant to non-uniform temperature for charge depleting conditions compared to the LFP cell group.

Because the changes in normalized discharge energy were relatively small some limitations of the test equipment are worth noting. First, the larger than unity cell group normalized energy for the NMC T_{avg}: 15°C/ ΔT: 5°C case at the C/2 and 1C rates may indicate that internal cell heating was able to increase the available energy by as much as 0.5%. This case is where the ΔT effect is smallest, and therefore the purest observation of the internal heating error magnitude. For the ΔT: 20°C and 1C rate this error may have been slightly stronger, which may explain the slope direction change for these cases.

Figure 13 presents the normalized EOD discharge energy profiles for both cell groups. Using the measured current profile for each cell in the group, and the total group voltage profile, the cumulative discharged energy for each cell was calculated for all tested conditions. Figure 13 provides a compressed set of the data, by only plotting the C/5 and 1C rates that were tested; leaving out the C/2 case for brevity. The presented energy profiles were normalized using the largest calculated discharge energy for a single cell across all of the tested conditions, which was at the 35°C average temperature and C/5-rate case (i.e., the case for the highest average temperature and lowest C-rate). The largest measured discharge energy for one of the 18650 cells in the LFP cell group was measured to be 4.53 Wh, and for the NMC cells this was 7.84 Wh. The horizontal axis indicates the cell position index within the cell group, where Cell 1 is the coldest cell, and Cell 5 is the hottest cell. This is also indicated in the upper right portion of Figure 13b.

For both cell groups the energy profiles are nonlinear in that the hotter cells did not improve in their contributed energy output in an equally matched amount as was lost by the colder cells. This resulted in the average output energy being reduced for increasing ΔT, and this explains the reduced bulk cell group output energy with increased ΔT that was presented in Figure 12. For example, in Figure 13b, looking at the NMC cell group and the ΔT:20°C case, the coldest cell output energy drops from the average by approximately 15%, while the hottest cell output energy increased by only about 10%. The total difference in output energy between the hottest and coldest cells follows closely with the measured ΔSOC that was presented in Figure 9.

The EOD energy profile for the LFP cell group experienced a disturbance which was most dramatic at higher average temperatures. In particular, Cell 4 generally produced more energy than Cell 5, which does not follow with the temperature profile, as Cell 4 was always cooler than Cell 5. This is likely explained by a slight cell-to-cell variation, which the LFP cells may be more sensitive to (due to flat OCV) than the NMC cells.

Next, a tolerable ΔT for each chemistry based on setting a specified allowable ΔSOC was extracted from the maximum ΔSOC data provided in the left column of Figure 9. A tolerable ΔT was interpolated for each average temperature and C-rate tested here. Figure 14 presents the maximum tolerable ΔT for cases where the maximum ΔSOC tolerance was set to 2% and 5%, in the top and bottom subplots, respectively. The 2% and 5% ΔSOC limits were admittedly selected somewhat arbitrarily, however, they serve to exemplify the methodology and appear to be reasonable limits. This information could be used to aid in guiding both thermal management system ΔT tolerances, as well as thermal management system control parameters.

From Figure 14, a substantial increase in the ΔT tolerance occurred as the average cell group temperature was increased from 15°C to 35°C. Additionally, we can see that the NMC cell group had a higher tolerance to thermal non-uniformity. This point is interesting as the opposite conclusion may have been drawn by comparing the *DCR* versus temperature sensitivity and/or the non-uniform temperature pulse test results. However, as the ΔU_{eq} effect provided a significant corrective action to reducing the development of ΔSOC the NMC cell group had an effectively lower sensitivity to thermal non-uniformity for the charge depleting use case. The designer must decide upon how much non-uniform *SOC* is tolerable, but from that one can then use this methodology to guide the tolerable ΔT for a thermal management system.

It is important to note that this chart is in regard to the effects of thermal non-uniformity that occurs across parallel connected cells.

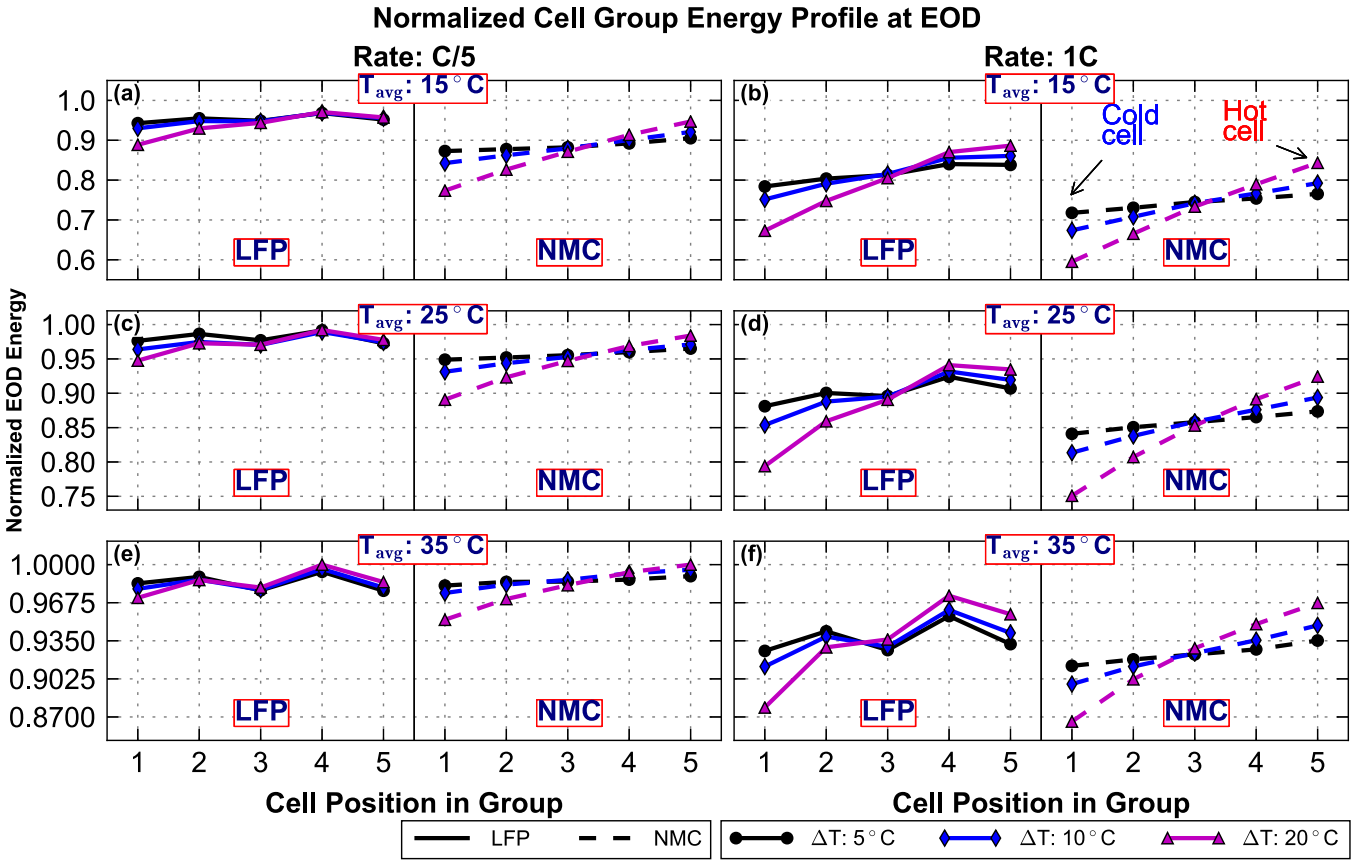

Figure 13. Comparison of the EOD normalized discharge energy profiles of all cells in the LFP and NMC cell groups. This is showing the effect that C-rate, average temperature, and ΔT have on the amount of discharge energy non-uniformity that occurs across the cell group. The energy profiles were normalized by the maximum calculated energy from all of the data in this figure. The maximum available discharge energy for a single 18650 LFP cell was 4.53 Wh, and 7.84 Wh for a NMC cell. This occurred at the high average temperature, and low C-rate condition in subplot (e).

This case is likely more tolerable to ΔTs due to the corrective action of the ΔU_{eq} effect. However, were thermal non-uniformity placed along serially connected cells this will not occur, as all cell groups will have the same *SOC*, due to current conservation through a series connection. In that case, a generally lower *DCR* temperature sensitivity (e.g., the LFP cells) would be less sensitive to ΔT.

Conclusions

Here we have studied the performance effects that non-uniform temperature has among parallel connected Li-ion cells. The difference in the thermal effect between short-time 10 sec current pulses and full capacity discharging was analyzed. These results were compared across two distinctly different and commercially important Li-ion cell chemistries; namely $LiFePO_4/C_6$ (LFP) and $LiNiMnCoO_2/C_6$ (NMC) in the 18650 form factor. The influence of the cell group average temperature, State of Charge (*SOC*), and C-rate was analyzed at varying levels of temperature non-uniformity.

For the 10 sec pulses, the current distribution that developed among the parallel connected cells followed the relative *DCR* versus temperature sensitivity. Conditions that increase the *DCR* versus temperature sensitivity increased the amount of current non-uniformity. For example, lower *SOC*, and lower average temperature had the strongest impact on increasing the sensitivity to non-uniform temperature for both chemistries. Lower rates had a subtle impact on this sensitivity, in that the charge transfer resistance is generally higher at lower rates. For the low rate, low *SOC*, low average temperature, and highest ΔT (i.e., highest degree of measured current non-uniformity) the hottest cell in the NMC cell group was required to carry nearly 1.8 times the average cell current. In contrast, the hottest cell in the LFP cell group was loaded to 1.4 times the average cell current. The NMC cells had a larger *DCR* versus temperature sensitivity compared to the LFP cells, and therefore the current non-uniformity was larger in the NMC cell group.

The results observed for the charge depleting testing were significantly different than the pulse testing, and this was primarily attributed to the development of non-uniform equilibrium potentials among the cells. Non-uniform equilibrium potentials developed due to the non-uniform *SOC*s that were caused by the sustained non-uniform current distribution. The development of non-uniform equilibrium potentials actually aided in unifying the current distribution, particularly when the magnitude of non-uniform equilibrium potential was of similar magnitude to the overpotential developed by the cell impedance. Due to the LFP chemistry having a moderately flat equilibrium potential this corrective action was not as strong compared to the NMC chemistry. This result was the reverse of what may have been presumed by the *DCR* versus temperature sensitivity and/or the non-uniform temperature pulse results.

The maximum non-uniform *SOC* that developed was a difference of 28% *SOC* between the coldest and hottest cells at the 1C rate and T_{avg}: 15°C/ ΔT: 20°C for the LFP cell group, while slightly lower at 26% for the NMC cell group. Due to the Arrhenius temperature sensitivity of the *DCR*, the maximum *SOC* non-uniformity at T_{avg}: 35°C/ ΔT: 20°C and 1C rate reduced to 16 and 11% for the LFP and NMC cell groups, respectively.

The discharge energy available at T_{avg}: 15°C/ ΔT: 20°C relative to T_{avg}: 15°C/ ΔT: 0°C for the C/2 rate case was reduced by 3%, which was the maximum reduction in available discharge energy relative to the respective uniform temperature case for all conditions tested here.

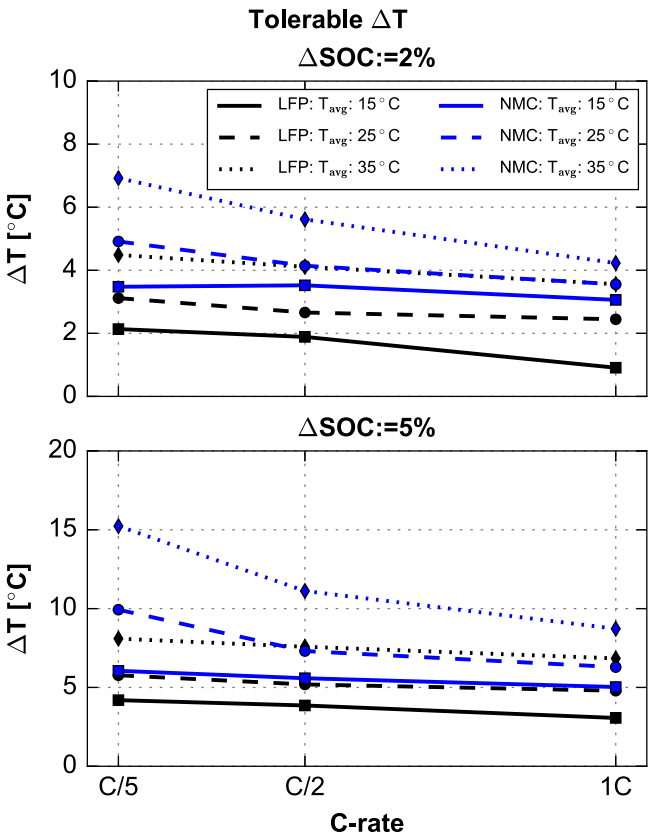

Figure 14. Interpolation of the maximum ΔSOC plot for set limits of ΔSOC of 2% (top) and 5% (bottom). Both cells are plotted, LFP (black) and NMC (blue).

Finally, it was shown that our results may be used to develop a guideline for the amount of tolerable ΔT for each cell chemistry given a specific limit to the allowable level of *SOC* non-uniformity. The tolerable ΔT has a significant sensitivity to both average temperature and discharge rate, which may be useful to account for in thermal management system control strategies. Based on both the discharge energy and tolerable ΔT results the NMC cell group was more tolerable to ΔT for a given *SOC* non-uniformity tolerance.

Acknowledgments

The authors kindly acknowledge Dr. Keith Kepler of Farasis Energy, Inc. for providing the NMC cells used in our study.

References

1. G. Kim, K. Smith, K. Lee, S. Santhanagopalan, and A. Pesaran, *Journal of The Electrochemical Society*, **158**, A955 (2011).
2. J. Yi, U. Kim, C. Shin, T. Han, and S. Park, *Journal of The Electrochemical Society*, **160**, A437 (2013).
3. T. Waldmann, G. Bisle, B. Hogg, S. Stumpp, M.A. Danzer, M. Kasper, P. Axmann, and M. Wohlfahrt-Mehrens, *Journal of The Electrochemical Society*, **162**, A921 (2015).
4. S. J. Bazinski and X. Wang, *Journal of The Electrochemical Society*, **161**, A2168 (2014).
5. M. Fleckenstein, O. Bohlen, M. A. Roscher, and B. Bker, *Journal of Power Sources*, **196**, 4769 (2011).
6. Y. Troxler, B. Wu, M. Marinescu, V. Yufit, Y. Patel, A. J. Marquis, N. P. Brandon, and G.J. Offer, *Journal of Power Sources*, **247**, 1018 (2014).
7. M. Klein, S. Tong, and J. W. Park, *Applied Energy*, **165**, 639 (2016).
8. J. B. Robinson, J. A. Darr, D. S. Eastwood, G. Hinds, P. D. Lee, P. R. Shearing, O. Taiwo, and D. Brett, *Journal of Power Sources*, **252**, 51 (2014).
9. C. Veth, D. Dragicevic, and C. Merten, *Journal of Power Sources*, **267**, 760 (2014).
10. D. R. Baker and M. W. Verbrugge, *Journal of The Electrochemical Society*, **146**, 2413 (1999).
11. B. Yan, C. Lim, L. Yin, and L. Zhu, *Journal of The Electrochemical Society*, **159**, A1604 (2012).
12. A. Ferrese and J. Newman, *Journal of The Electrochemical Society*, **161**, A948 (2014).
13. N. Baba, H. Yoshida, M. Nagaoka, C. Okuda, and S. Kawauchi, *Journal of Power Sources*, **252**, 214 (2014).
14. Y. Dai, L. Cai, and R. E. White, *Journal of The Electrochemical Society*, **161**, E3348 (2014).
15. M. Xu, Z. Zhang, X. Wang, L. Jia, and L. Yang, *Journal of Power Sources*, **256**, 233 (2014).
16. P. Taheri, A. Mansouri, B. Schweitzer, M. Yazdanpour, and M. Bahrami, *Journal of The Electrochemical Society*, **160**, A1731 (2013).
17. S. Allu, S. Kalnaus, W. Elwasif, S. Simunovic, J.A. Turner, and S. Pannala, *Journal of Power Sources*, **246**, 876 (2014).
18. T. Bandhauer, S. Garimella, and T. F. Fuller, *Journal of The Electrochemical Society*, **162**, A125 (2015).
19. S. Pannala, J. A. Turner, S. Allu, W. R. Elwasif, S. Kalnaus, S. Simunovic, A. Kumar, J. J. Billings, H. Wang, and J. Nanda, *Journal of Applied Physics*, **118**, 072017 (2015).
20. B. Wu, Z. Li, and J. Zhang, *Journal of The Electrochemical Society*, **162**, A181 (2015).
21. C. Veth, D. Dragicevic, R. Pfister, S. Arakkan, and C. Merten, *Journal of The Electrochemical Society*, **161**, A1943 (2014).
22. A. Awarke, S. Pischinger, and J. Ogrzewalla, *Journal of The Electrochemical Society*, **160**, A172 (2013).
23. M. Guo and R.E. White, *Journal of Power Sources*, **221**, 334 (2013).
24. M. Guo, G. Kim, and R.E. White, *Journal of Power Sources*, **240**, 80 (2013).
25. D.A.H. McCleary, J.P. Meyers, and B. Kim, *Journal of The Electrochemical Society*, **160**, A1931 (2013).
26. S. V. Erhard, P. J. Osswald, J. Wilhelm, A. Rheinfeld, S. Kosch, and A. Jossen, *Journal of The Electrochemical Society*, **162**, A2707 (2015).
27. N. Yang, X. Zhang, B. Shang, and G. Li, *Journal of Power Sources*, **306**, 733 (2016).
28. G. Zhang, C. E. Shaffer, C. Wang, and C. D. Rahn, *Journal of The Electrochemical Society*, **160**, A610 (2013).
29. G. Zhang, C. E. Shaffer, C. Wang, and C. D. Rahn, *Journal of The Electrochemical Society*, **160**, A2299 (2013).
30. P. J. Osswald, S. V. Erhard, J. Wilhelm, H. E. Hoster, and A. Jossen, *Journal of The Electrochemical Society*, **162**, A2099 (2015).
31. D. Andre, M. Meiler, K. Steiner, Ch. Wimmer, T. Soczka-Guth, and D. U. Sauer, *Journal of Power Sources*, **196**, 5334 (2011).
32. J. Schmidt, T. Chrobak, M. Ender, J. Illig, D. Klotz, and E. Tiff, *Journal of Power Sources*, **196**, 5342 (2011).
33. C. Wang, A. Appleby, and F. E. Little, *Electrochimica Acta*, **46**, 1793 (2001).
34. M. Itagaki, N. Kobari, S. Yotsuda, K. Watanabe, S. Kinoshita, and M. Ue, *Journal of Power Sources*, **135**, 255 (2004).
35. M.C. Smart, J.F. Whitacre, B.V. Ratnakumar, and K. Amine, *Journal of Power Sources*, **168**, 501 (2007).
36. X. Qiu, Q. Zhuang, Q. Zhang, R. Cao, Y. Qiang, P. Ying, and S. Sun, *Journal of Electroanalytical Chemistry*, **688**, 393 (2013).
37. D.W. Abarbanel, K.J. Nelson, and J.R. Dahn, *Journal of The Electrochemical Society*, **163**, A522 (2016).
38. S. Zhang, K. Xu, and T. R. Jow, *Electrochimica Acta*, **49**, 1057 (2004).
39. S.L. Wu, W. Zhang, X. Song, A. K. Shukla, G. Liu, V. Battaglia, and V. Srinivasan, *Journal of The Electrochemical Society*, **159**, A438 (2012).
40. L. Valoen and J. N. Reimers, *Journal of The Electrochemical Society*, **152**, A882 (2005).
41. J. Marcicki and X. G. Yang, *Journal of The Electrochemical Society*, **161**, A1794 (2014).
42. S. J. Bazinski and X. Wang, *Journal of The Electrochemical Society*, **161**, A168 (2014).
43. J. Sun, G. Wei, L. Pei, R. Lu, K. Song, C. Wu, and C. Zhu, *Energies*, **8**, 4400 (2015).
44. J. Huang, Z. Li, B. Y. Liaw, Z. Wang, S. Song, N. Wu, and J. Zhang, *Journal of The Electrochemical Society*, **162**, A2367 (2015).
45. F. Yun, W. Jin, L. Tang, W. Li, J. Pang, and S. Lu, *Journal of The Electrochemical Society*, **163**, A639 (2016).
46. M. J. Brand, M. H. Hofmann, M. Steinhardt, S. F. Schuster, and A. Jossen, *Journal of Power Sources*, **334**, 202 (2016).
47. P. J. Osswald, S. V. Erhard, A. A. Noel, P. P. Keil, F. M. Kindermann, H. H. Hoster, and A. Jossen, *Journal of Power Sources*, **314**, 93 (2016).
48. P. J. Osswald, S. V. Erhard, A. Rheinfeld, B. Rieger, H.E. Hoster, and A. Jossen, *Journal of Power Sources*, **329**, 546 (201).
49. S. V. Erhard, P. J. Osswald, P. Keil, E. Hffer, M. Haug, A. Noel, J. Wilhelm, B. Rieger, K. Schmidt, S. Kosch, F. M. Kindermann, F. Spingler, H. Kloust, T. Thoennessen, A. Rheinfeld, and A. Jossen, *Journal of The Electrochemical Society*, **164**, A6324 (2017).
50. A. Marongiu and D. U. Sauer, *International Journal of Automotive Technology*, **17**, 465 (2016).
51. A. Sakti, J. Michalek, S. Chun, and J. F. Whitacre, *International Journal of Energy Research*, **37**, 1562 (2013).